This is a preprint, the final version is subject to change, of the American Mineralogist (MSA)
Cite as Authors (Year) Title. American Mineralogist, in press.
(DOI will not work until issue is live.) DOI: http://dx.doi.org/10.2138/am.2014.4612

Revision 1

Solid phases of FeSi to 47 GPa and 2800 K

Zachary M. Geballe and Raymond Jeanloz

Department of Earth and Planetary Sciences, University of California,

Berkeley, CA, 94720, U.S.A.

Abstract

FeSi remains crystalline up to at least 2350 (± 200) K at 23 GPa and 2770 (± 200) K at 47 GPa in a laser-heated diamond anvil cell, showing that addition of silicon does not cause a large amount of melting point depression (the melting temperature of pure iron ranges from 2300 (± 100) K to 2700 (± 150) K between 20 and 50 GPa). The transition between ε (B20) and B2 (CsCl-structured) crystalline phases occurs at 30 (± 2) GPa at all temperatures from 1200 K to 2400 K. The resulting 5% density increase may cause an increase in the miscibility of silicon in iron at $P > 30$ GPa, with potential implications for the cores of small rocky planets such as Mars and Mercury.

Introduction

Equations of state, melting curves, mixing relations and solid-solid phase boundaries in iron and its alloys are the key equilibrium properties needed for modeling the constitution and evolution of planetary cores. Silicon is one element that is likely to be alloyed with iron in the cores of rocky planets; it is abundant in the rocks found on the surfaces of Mercury, Venus, Earth and Mars (de Pater and Lissauer 2010), and in the laboratory it is known to alloy with liquid iron at high pressures (Sanloup and Fei 2004) or at low oxygen fugacity (McCoy et al.

1999).

Recently, the cubic ε-phase (B20) of FeSi was found to transform to another cubic phase, B2 (CsCl-structured), at 24 GPa and high temperature (Dobson et al. 2002): conditions that exist in the cores of Mars and Mercury. Some thermodynamic properties of these phases have been documented, but others remain uncertain.

Experimental studies have determined the P-V equation of state of ε-FeSi (Lin et al. 2003; Knittle and Williams 1995), and of B2-FeSi (Dobson et al. 2003; Sata et al. 2010), in addition to iron-rich iron-silicon alloys (Asanuma et al. 2011; Fisher et al. 2012). A computational study using DFT with GGA derived equations of state that are similar to the experimental result, though slightly stiffer: for B2-FeSi, the zero-pressure bulk modulus is 9% higher than in Sata et al. (2010); and for ε-FeSi, the pressure derivative of bulk modulus is 7% higher than in Lin et al. (2003) (Caracas and Wentzcovitch 2004). The computational work also estimated the ε-B2 transition pressure: 40 GPa assuming a GGA functional, and 30 GPa assuming the LDA functional (Caracas and Wentzcoitch 2004). Yet, less experimental data exists to constrain the transition pressure and its temperature dependence.

The density and entropy changes due to the crystal-crystal phase transition are expected to affect the melting curves of iron-silicon alloys, as well as their mixing relations. In fact, one experimental study associates a kink in the melting curve of FeSi to the solid-solid phase transition (Santamaría-Pérez and Boehler 2008), though a second study of melting in diamond anvil cells infers a melting curve of FeSi that is ~500 K higher and shows no kink (Lord et al. 2010). Most recently, Fisher et al. 2013 mapped out phase boundaries for FeSi up to 150 GPa using a laser-heated diamond anvil cell, casting doubt on the melting curve of Santamaría-Pérez and Boehler (2008), and providing high-quality diffraction data that suggest an extended region of mixed phase between ε and B2, from 14 to 42 GPa.

By varying the composition of their starting materials, two studies provide evidence for miscibility gaps between pure iron and FeSi. Kuwayama and Hirose (2004) detects a gap from 37 to 50 mol% Si at 21 GPa while Lin et al. (2002) detects a gap from 10 to 20 mol% Si in the pressure range of 11 to 42 GPa.

The current study adds new data on stoichiometric FeSi that tightly constrain the ε to B2 phase boundary, provide a lower bound on the melting curve, and confirm previously proposed equations of state that indicate a 5% density increase due to the phase transition.

Experimental method

Stoichiometric FeSi was synthesized and given to us by Ravhi S. Kumar. It was ground to a powder, pressed into a thin foil, and placed on top of ruby spheres into diamond anvil cells with rhenium gaskets. The samples were surrounded with an argon or neon pressure transmitting medium, which was loaded at room temperature and 25,000 PSI using the system at GSECARS (Rivers et al. 2008).

High-pressure samples were laser-heated at GSECARS end-station ID-D, and simultaneous emission spectra and X-ray diffraction images were collected (Prakapenka et al. 2008). The X-ray wavelength was 0.33 Å and the sample to detector distance was 200 mm. By looking at the relative position of the two laser spots (one from each side) and fluorescence from the X-ray spot before and after heating, we estimate that the centers of all three beams were within 3 μm of each other. Laser-heating hotspots are at least ~10 μm wide at FWHM of emission intensity. Since intensity scales as T^4, the FWHM of the temperature distribution of the hotspot is ~40 μm, meaning a 3 μm deviation causes less than ~5% error in temperature, assuming a Gaussian temperature distribution.

X-ray exposure times ranged from 1 to 5 seconds, while temperature measurement times ranged from 5 ms to 1 s. The temperatures reported here are averages of at least two exposures during the X-ray experiment. The 1-σ temperature uncertainties plotted in Fig. 1 are standard deviations of at least four fitted temperatures, which come from the two sides of the sample and the two or more thermal emission records collected during a single X-ray exposure. The statistical uncertainty in fitting greybody curves to collected emission spectra can be ignored, as it is typically less than 10 K. We do not attempt to quantify temperature uncertainty due to deviations from greybody behavior (Benedetti and Loubeyre 2004). At the highest recorded temperatures, the temperature varied by ~150 K between X-ray exposures. For example, after increasing laser power, temperature typically decreased in the subsequent ~10 seconds required to collect two diffraction patterns. Combining this 150 K variability with the ≤ 5% uncertainty due to misalignment of the X-ray beam with hotspot gives a conservative estimate of uncertainty in the data used to constrain the lower bound on the melting curve: ± 200 K.

Pressures were determined from ruby fluorescence, and from the neon and argon equations of state (Fei et al. 2007; Errandonea et al. 2006). At select points, we confirm that

the pressures determined from the noble gas solids match the ruby pressures to within 0.5 GPa. The pressure increase upon heating was estimated to be 2.2 ± 0.8 GPa by using select measurements within the neon medium, the neon P-V-T equation of state (Fei et al. 2007) and by assuming the average temperature of neon is half that of the sample. The pressure changed from before heating to after heating by 0 to 2 GPa, depending on the heating run, with a typical change of 0.9 GPa. We combine these two sources of uncertainty in pressure by adding them in quadrature, resulting in a typical pressure uncertainty of ±1.2 GPa.

Results

The solid-solid phase transition from the low-pressure ε phase to the high-pressure B2 phase of FeSi occurs at 30±2 GPa, the weighted average of the transition pressures detected in a neon pressure medium (31.2±1.7 GPa) and in an argon medium (28±1.9 GPa) (Fig. 1). The quoted uncertainties in pressure for each medium are the quadrature sums of two errors: the typical pressure uncertainty of any given data point (±1.2 GPa) and the uncertainty in bracketing the transition upon compression and decompression, given those data points. The bracketing uncertainty in the neon is half the difference from highest-pressure phase to lowest-pressure B2 phase, while the bracketing uncertainty in the argon medium is calculated using the statistical method of Kavner et al. (2000). It includes hysteresis due to kinetics of the transition as well as the number of distinct pressures at which measurements were made.

We detected no temperature dependence of the ε-B2 transition in either pressure medium, despite controlling the temperature at 1200 ± 100 K for tens of seconds before increasing laser power: either the sample started transforming immediately upon heating to 1200 K, or it did not transform until pressure was increased. This is consistent with the data of Fisher et al. (2013), which was used to infer a steep slope of the boundary between their mixed phase region and B2 region: $\left|\frac{dT}{dP}\right| \geq 180$ K/GPa.

The ε-B2 transition was reversed multiple times in each pressure medium. Examples of X-ray diffraction spectra that evidence the transition are shown in Fig. 2. To constrain the hysteresis of the phase transition, we reversed the transition four times in a cell containing the

neon pressure medium, and twice in a cell containing the argon medium. The reversals in neon showed no evidence of hysteresis once they were laser-heated, but rather bracket the transition to between 30 and 32.3 GPa. The reversals in argon, on the other hand, show hysteresis: upon laser-heating, the B2 phase is created at 32 GPa, transformed into the ε phase at 23 GPa on decompression, and transformed back into the B2 phase at 30 GPa upon re-compression. The difference in hysteresis observed for neon versus argon is likely due to the differing stress states created by the two pressure media, perhaps with deviatoric stress helping to overcome kinetic barriers, but the mechanism is not known.

X-ray diffraction patterns of samples at room temperature provide data to constrain the P-V equation of state of both phases of FeSi. Fig. 3 shows that our data are well-described by previously published equations of state of ε-FeSi (Lin et al. 2003) and of B2-FeSi (Sata et al. 2010), whereas the volumes of metastable B2-FeSi at less than 23 GPa are lower than those predicted by the equation of state of Dobson et al. (2003). P-V data from all studies indicate a 5% density increase at 30 GPa.

Discussion

The regions of stability of ε and B2 solid phases of FeSi are consistent with some but not all previously published high-pressure, high-temperature data. First, Fig. 4 shows that our observations of X-ray diffraction peaks from solid FeSi give a lower bound on the melting curve that is >200 K higher than the melting curve of Santamaría-Pérez and Boehler (2008) from ~7 to 18 GPa, showing that the laser-speckle method yields anomalously low temperatures in this case. In contrast, the melting curve determined by identifying kinks in temperature vs. laser power is sufficiently high to be consistent with our data (Lord et al. 2010). However, recent analysis of temperature evolution in laser-heated diamond cells shows that any kinks in temperature as a function of laser power cannot be ascribed to the latent heat of melting, but may instead be related to changes in optical properties or thermal conductivity of the sample or insulation (Geballe and Jeanloz 2012). In addition, in the appendix we show the lack of any kink near 30 GPa in the melting curve of Lord et al. (2010) is inconsistent with the 5% volume collapse documented in the present study.

The location of the triple point was previously inferred to be at less than 20 GPa and between 1500 to 2200 K. In one study, the location was based on a kink in the melting curve (Santamaría-Pérez and Boehler 2008), while in the other it was based on diffraction spectra of

pressure- and temperature-quenched samples (Lord et al. 2010), and reinforced by the multi-anvil data of Dobson et al. (2002). More recently, Fisher et al. (2013) infer a triple point at ~ 42 GPa and 3000 K, but in this case, the low-pressure low-temperature region is a solid solution of B2 and ε phases. In contrast, our data suggest a triple point at ~30 GPa. Assuming the transition pressure determined here, the discrepancy with the earlier data may be due to ambiguity in the interpretation of laser-speckle, and uncalibrated pressure change upon heating in the multi-anvil experiments of Dobson et al. (2002). The low-pressure samples that were seen to be partially converted from ε to B2 phase in the quenched diamond-cell experiments of Lord et al. (2010) are harder to reconcile with our proposed phase diagram. The cause of the discrepancy may be due to the different pressure media used (Al_2O_3 versus argon and neon in this study) or due to the difference in pressure-temperature paths (diffraction on quenched samples versus the in- situ measurements presented here). Alternatively, the temperature stability and accuracy of measurement in the present study may be insufficient to resolve the temperature dependence of the phase transition.

The disagreement with Fisher et al. (2013) is subtler: we do not see evidence that the ε phase is stable above 30 GPa (e.g. Fig. 2), whereas they detect diffraction peaks due to the ε phase at pressures up to 42 GPa but with peak intensities diminishing with pressure. It is possible that a misalignment between laser and X-ray beams allowed remnant ε-FeSi to remain metastable in the previous work, and that part of the probed sample was not heated enough to overcome a kinetic barrier to the phase transition. Stronger evidence of a mixed-phase region is the observation of Fisher et al. (2013) that small amounts of the B2 phase are mixed into the majority ε phase between 14 and 30 GPa. Although we see no evidence of this in our data, our crystal sizes may have been larger, causing poorer-quality powder diffraction, hence an inability to identify the B2 phase. We conclude that the mixed phase region proposed by Fisher et al. (2013) is possible but not yet confirmed by independent study.

Lower bounds on the melting curve reinforce previous arguments that addition of silicon causes little melting point depression (e.g. Morard et al. 2011, Fisher et al. 2013). A compilation of melting point measurements and ab- initio calculations shows that the melting curve of pure iron ranges from 2300 ± 100 K to 2700 ± 150 K between 20 and 45 GPa (Li and Fei 2013), whereas our data indicate a lower bound on the melting curve of FeSi of 2300 K at these pressures. This suggests that silicon causes a melting point depression of less than ~16%,

consistent with the estimate of Morard et al. (2011) of ~10% melting point depression, and reinforcing their conclusion that addition of sulfur, a different light element that they also studied, has a larger effect.

The 5% density increase due to phase transformation of the FeSi compound upon pressure increase may have implications for the cores of Mercury (P_{core}~10 to 40 GPa) and/or Mars (P_{core}~24 to 40 GPa) if silicon is an abundant alloying element (de Pater and Lissauer 2010). Qualitatively, the miscibility of silicon in crystalline iron may increase at ~30 GPa due to the increase in the effective hard-sphere radius of silicon in the FeSi lattice as its coordination changes from 7-fold (ε-phase) to 8-fold (in the B2 structure), thereby improving the similarity of the radii of silicon and iron. Specifically, the immiscibility gap documented between iron-rich and iron-poor iron-silicon alloys at < 50 mol% Si may be reduced at pressures above 30 GPa.

Implications

X-ray diffraction experiments on laser-heated FeSi in a diamond cell show that the transition from ε- to B2-FeSi takes place at 30 ± 2 GPa, with no detectable temperature dependence. The corresponding 5% volume collapse and increase in coordination of silicon from 7-fold to 8-fold may cause increased miscibility of silicon in crystalline iron at the pressure-temperature conditions inside the cores of Mercury and Mars.

Acknowledgements

We thank Ravhi Kumar the sample material, Laura Robin Benedetti for help designing the study, and Sergey Tkachev and Vitali Prakapenka for help loading the samples. We acknowledge the support of GeoSoilEnviroCARS (Sector 13), which is supported by the National Science Foundation - Earth Sciences (EAR-1128799), and the Department of Energy, Geosciences (DE-FG02-94ER14466). Use of the Advanced Photon Source, an Office of Science User Facility operated for the U.S. Department of Energy (DOE) Office of Science by Argonne National Laboratory, was supported by the U.S. DOE under Contract No. DE-AC02-06CH11357. Support for Z. M. G. was provided in part by an NSF Graduate Fellowship.

Appendix

In this appendix we apply the Clausius-Clapeyron relation three times and use the slope of the solid-solid phase transition determined here to find this useful expression for the change in slope of the melting curve at 30 Gpa:

$$\left.\frac{\frac{dT}{dP}\Big|_{+}}{\frac{dT}{dP}\Big|_{-}} \geq \left(1+\frac{\left(V_\varepsilon - V_{B2}\right)/V_\varepsilon\big|_{30GPa}}{\left(V_l - V_\varepsilon\right)/V_\varepsilon\big|_{0GPa}}\right)\right/ 1.06 \qquad (1)$$

Next, we apply the Clausius-Clapeyron equation once again to find the volume change upon melting at 0 GPa: we take the product of the Clapeyron slope from Lord et al. (2010), 50 K/GPa, the entropy of fusion from Zaitsev et al. (1991), 18 J/mol K, and the density, 0.08 mol/cm^3, to find $\left(V_l - V_\varepsilon\right)/V_\varepsilon\big|_{0GPa} = \Delta V \Big/ V_\varepsilon = \Delta S \frac{dT}{dP}\rho_\varepsilon = 0.07$. Since our data confirms the volume change of the crystal-crystal phase transition to be 5%, expression (1) is $(1+0.05/0.07)/1.06 = 1.6$, meaning we expect the slope of the melting curve of Lord et al. (2010) to change by at least 60% at the ε-B2-liquid triple point, a change well within the precision of the published melting curve, which shows no such kink.

Now we derive equation (1). Applying the Clapeyron relation to the slopes of the melting curve just above and just below the triple point, we find the ratio of slopes is

$$\left.\frac{\frac{dT}{dP}\Big|_{+}}{\frac{dT}{dP}\Big|_{-}} = \frac{\Delta V_{l/B2}}{\Delta S_{l/B2}} \Big/ \frac{\Delta V_{l/\varepsilon}}{\Delta S_{l/\varepsilon}} = \frac{V_l - V_{B2}}{V_l - V_\varepsilon} \Big/ \frac{S_l - S_{B2}}{S_l - S_\varepsilon}\right.$$

$$= \frac{V_l - V_\varepsilon + V_\varepsilon - V_{B2}}{V_l - V_\varepsilon} \Big/ \frac{S_l - S_\varepsilon + S_\varepsilon - S_{B2}}{S_l - S_\varepsilon}$$

$$= \left(1+\frac{V_\varepsilon - V_{B2}}{V_l - V_\varepsilon}\right) \Big/ \left(1+\frac{S_\varepsilon - S_{B2}}{S_l - S_\varepsilon}\right) \qquad (2)$$

Whereas this equation is exact at the triple point, we make two approximations to allow use of data at ambient pressure. Since liquids are typically more compressible than solids, the fractional change in volume upon melting at 30 GPa is less than the change at 0 GPa,

meaning the numerator of expression (2) is at least $\left(1+\frac{\left(V_\varepsilon - V_{B2}\right)/V_\varepsilon\big|_{30GPa}}{\left(V_l - V_\varepsilon\right)/V_\varepsilon\big|_{0GPa}}\right)$ The denominator of (2) is approximately 1, because the boundary between ε and B2 phases is nearly vertical. Assuming the shallowest slope our data allow, 1200 K over 2 GPa (Fig. 1), a third use of the Clausius- Clapeyron relation yields a change in entropy of 1.1 J/mol K, which is ~6% of the entropy of fusion reported by Zaitsev et al. (1991) at ambient pressure, making the denominator of expression (2) at most ~1.06. Substitution of both numerator and denominator yields equation (1).

References cited

Asanuma, H., Ohtani, E., Sakai, T., Terasaki, H., Kamada, S., Kondo, T., and Kikegawa, T. (2010) Melting of iron silicon alloy up to the core mantle boundary pressure: implications to the thermal structure of the Earths core. Physics and Chemistry of Minerals, 37, 353–359.

Benedetti, L. R. and Loubeyre, P. (2004) Temperature gradients, wavelength-dependent emissivity, and accuracy of high and very-high temperatures measured in the laser-heated diamond cell. High Pressure Research, 24, 423–445.

Caracas, R. and Wentzcovitch, R. (2004) Equation of state and elasticity of FeSi. Geophysical Research Letters, 31, L20603.

de Pater, I. and Lissauer, J. J. (2010) Planetary Sciences, 2nd ed. (Cambridge University Press, New York).

Dobson, D. P., Vocadlo, L. and Wood, I. G. (2002) A new high-pressure phase of FeSi. American Mineralogist, 87, 784–787.

Dobson, D. P., Crichton, W. A., Bouvier, P., Vocadlo, L. and Wood, I. G. (2003) The equation of state of CsCl-structured FeSi to 40 GPa: Implications for silicon in the Earth's core. Geophysical Research Letters, 30, 1014.

Errandonea, D., Boehler, R., Japel, S., Mezouar, M., and Benedetti, L. (2006) Structural transformation of compressed solid Ar: An x-ray diffraction study to 114 GPa. Physical Review B, 73, 092106.

Fei, Y., Ricolleau, A., Frank, M., Mibe, K., Shen, G., and Prakapenka, V. (2007) Toward an internally consistent pressure scale. Proceedings of the National Academy of Sciences of the United States of America, 104, 9182–6.

Fischer, R. A., Campbell, A. J., Caracas, R., Reaman, D. M., Dera, P. and Prakapenka, V. B. (2012) Equation of state and phase diagram of Fe-16Si alloy as a candidate component of Earth's core. Earth and Planetary Science Letters, 357-358, 268–276.

Fischer, R. A., Campbell, A. J., Reaman, D. M., Miller, N. A., Heinz, D. L., Dera, P., Prakapenka, V. B. (2013) Phase relations in the Fe-FeSi system at high pressures and temperatures. Earth and Planetary Science Letters, 373, 54-64.

Knittle, E. and Williams, Q., (1995) Static compression of ε-FeSi and an evaluation of reduced silicon as a deep Earth constituent. Geophysical Research Letters, 22, 445–448.

Kuwayama, Y. and Hirose, K. (2004) Phase relations in the system Fe-FeSi at 21 GPa. American Mineralogist, 89, 273–276.

Li, J., and Fei, Y., (2013) Experimental Constraints on Core Composition. In Treatise on Geochemistry, Vol. 3, edited by K. K. Turekian and H. D. Holland (Cambridge University Press, New York) 2nd ed., Chap. 3.

Lin, J.-F., Campbell, A. J., Heinz, D. L., and Shen, G. (2003) Static compression of iron-silicon alloys: Implications for silicon in the Earth's core. Journal of Geophysical Research, 108, 2045.

Lin, J.-F. , Heinz, D. L., Campbell, A. J., Devine, J. M, and Shen, G. (2002) Iron-silicon alloy in Earth's core? Science, 295, 313–5.

Lord, O. T., Walter, M. J., Dobson, D. P., Armstrong, L., Clark, S. M., and Kleppe, A. (2010) The FeSi phase diagram to 150 GPa. Journal of Geophysical Research, 115, B06208.

McCoy, T. J., Dickinson, T. L., and Lofgren, G. E. (1999) Partial melting of the Indarch (EH4) meteorite: A textural, chemical, and phase relations view of melting and melt migration. Meteoritics and Planetary Science, 746, 735–746.

Morard, G., Andrault, D., Guignot, N., Siebert, J., Garbarino, G., and Antonangeli, D. (2011) Melting of FeNiSi and FeNiS alloys at megabar pressures: implications for the core-mantle boundary temperature. Physics and Chemistry of Minerals, 38, 767–776.

Prakapenka, V. B., Kubo, A., Kuznetsov, A., Laskin, A., Shkurikhin, O., Dera, P., Rivers, M. L., and Sutton, S. R. (2008) Advanced flat top laser heating system for high pressure research at GSECARS: application to the melting behavior of germanium. High Pressure Research, 28, 225–235.

Rivers, M., Prakapenka, V. B., Kubo, A., Kuznetsov, A., Pullins, C., Holl, C. M., and Jacobsen, S. D. (2008) The COMPRES/GSECARS gas-loading system for diamond anvil cells at the Advanced Photon Source. High Pressure Research, 28, 273–292.

306 Sanloup, C., and Fei, Y. (2004) Closure of the Fe-S-Si liquid miscibility gap at high pressure.
307 Physics of the Earth and Planetary Interiors, 147, 57–65.
308 Santamaría-Pérez, D., and Boehler, R. (2008) FeSi melting curve up to 70 GPa. Earth and
309 Planetary Science Letters, 265, 743-747.

310

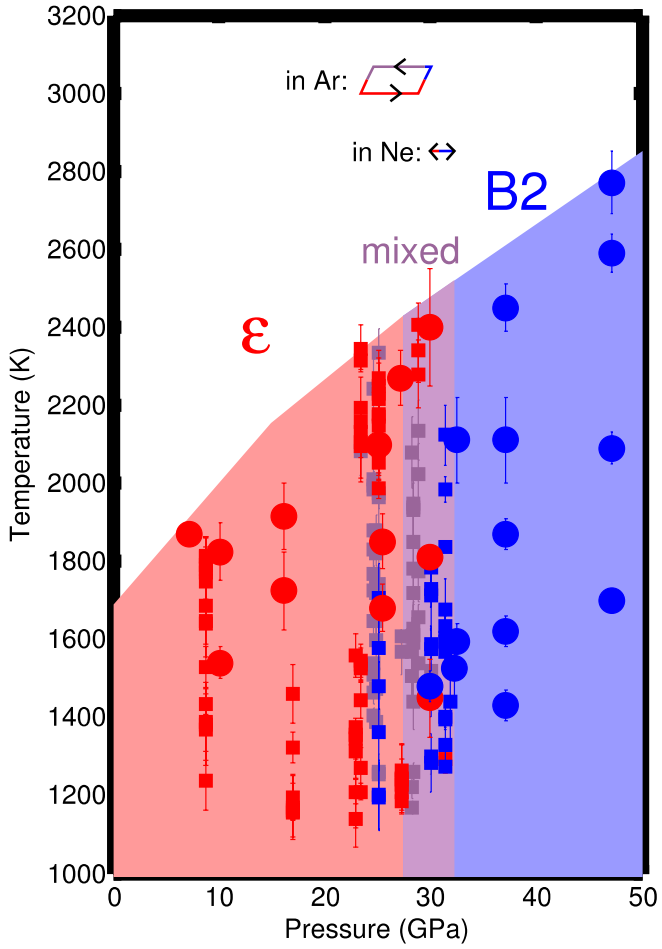

311

312

313

314 FIG. 1. The ε-B2 phase transition of FeSi occurs at 30 ± 2 GPa, with no detectable
315 temperature dependence between 1000 and 2400 K. Data using an argon pressure medium are
316 represented by squares. Red symbols represent ε-FeSi, blue represents B2-FeSi, and purple
317 indicates that a mixture of the two phases is seen in the diffraction data. Overlapping of
318 squares of various colors results from the hysteresis of the phase transition, revealed by
319 reversing the transition multiple times. The phase boundary and hysteresis are summarized by
320 the loop between 23 and 30 GPa, shown at the top of the figure. Data using a neon medium
321 are represented by circles and summarized by the double-headed arrow from 30 to 32.3 GPa

that indicates no observed hysteresis within our pressure intervals. Temperature uncertainties are indicated for each data point, whereas the typical pressure uncertainty for all data is estimated to be 1.2 GPa. All data plotted here are listed in a table available online.

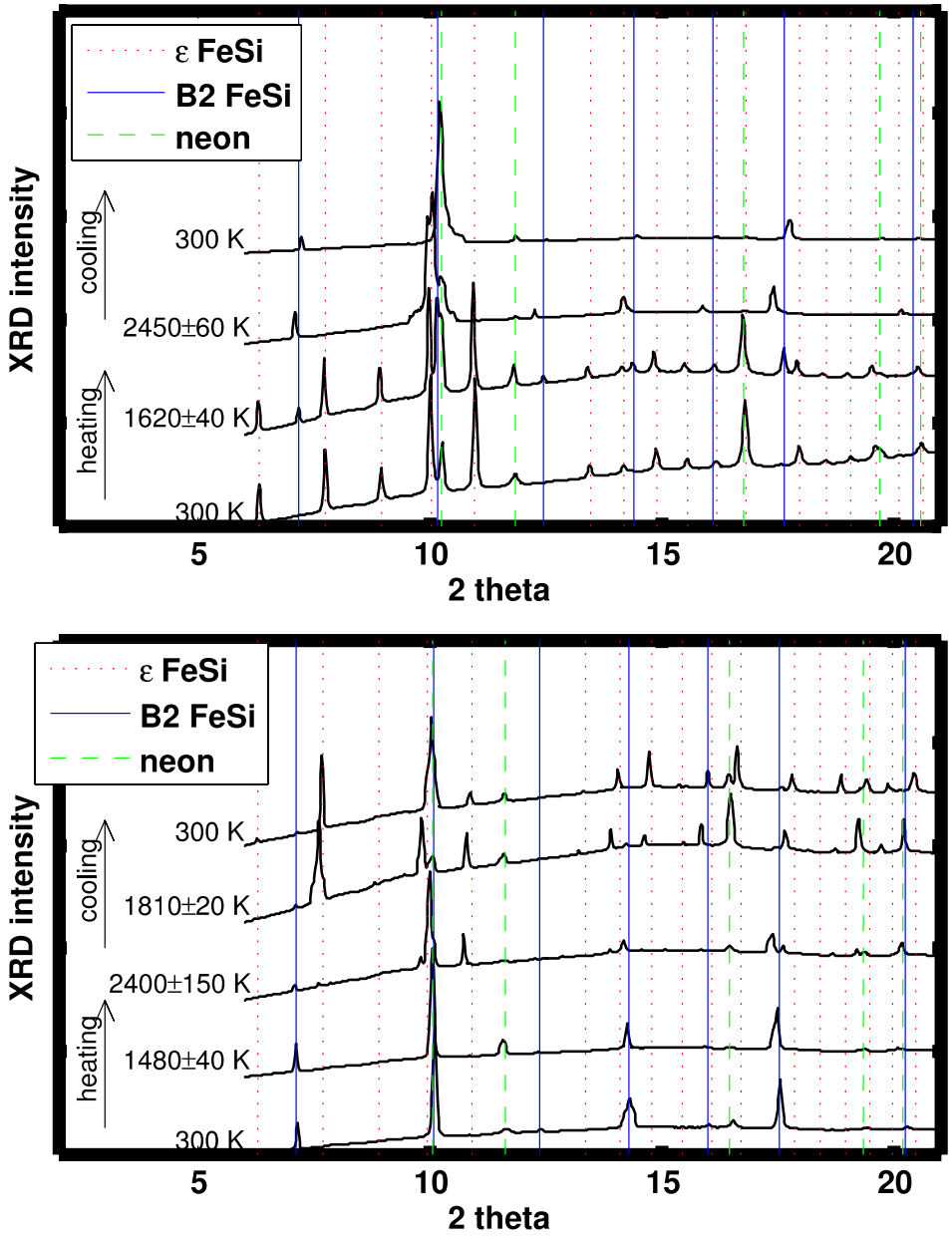

FIG. 2. Examples of diffraction patterns show a transition from the ε to the B2 phase of FeSi at 37 GPa (top) and the reverse transition, from B2 to ε at 30 GPa (bottom). Black curves show integrated powder diffraction data during the two heating/cooling cycles. Temperatures measured by spectroradiometry are shown to the left of diffraction patterns. Red dotted lines mark diffraction peak positions of ε-FeSi lattice planes at 37 GPa or 30 GPa, while blue solid lines mark positions of B2-FeSi lattice planes and green dashed lines mark positions of neon

lattice planes. Deviations of high-temperature diffraction peaks from theoretical peak positions are mostly due to thermal expansion of the sample and pressure medium.

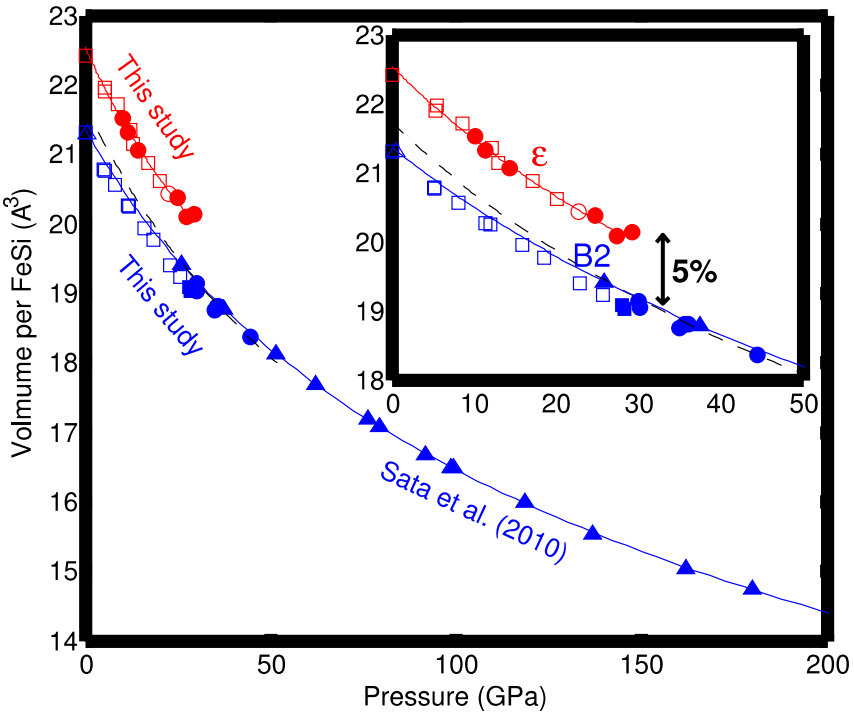

FIG. 3. Room temperature equation of state data for the ε and B2 phases of FeSi. Squares and circles represent argon and neon pressure media, while open and closed symbols represent data collected upon decompression and upon compression, respectively. The B2 phase is metastable upon decompression in the absence of laser-heating, as shown by the open squares from 0 to 23 GPa. Blue triangles are data from Sata et al. (2010). Red, blue and black dashed curves show equations of state from Lin et al. (2003), Sata et al. (2010), and Dobson et al. (2003), respectively

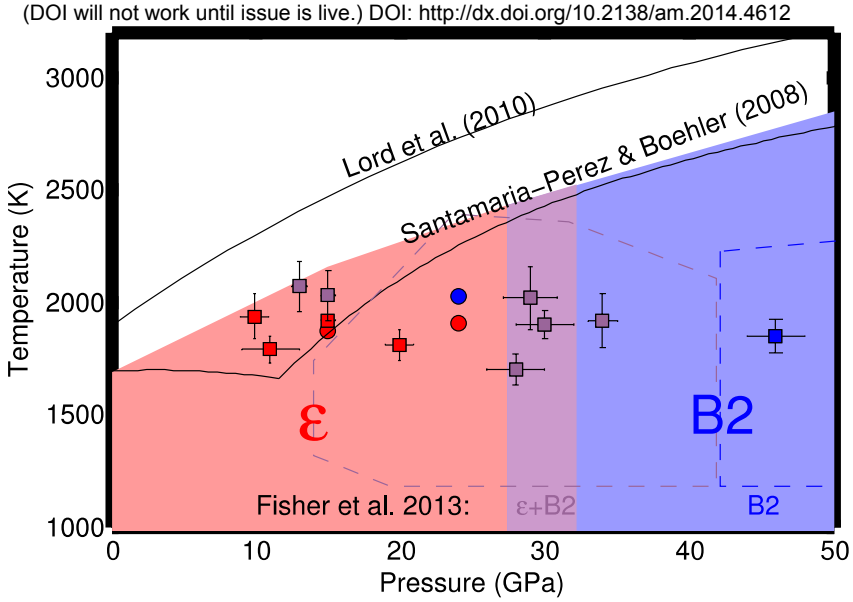

346

347

348 FIG. 4. Phase boundaries determined in the present study are compared with solid phases and
349 melting transitions identified in previous studies. Lines indicate melting curves. Squares and
350 circles indicate crystalline structures documented in Lord et al. (2010) and in Dobson et al.
351 (2002), respectively. Purple symbols indicate both crystalline phases were detected. Red, blue
352 and purple shading mark regions of ε, B2 and mixed phase stability in the current study. The top
353 of the shaded region represents the lower bound on the melting curve in the present study. The
354 uncertainty in this lower bound is at most ± 200 K. Purple and blue dashes outline phase fields
355 identified in Fisher et al. (2013).